CrossMark
click for updates



# Novel protein Callipygian defines the back of migrating cells

Kristen F. Swaney[a], Jane Borleis[a], Pablo A. Iglesias[a,b], and Peter N. Devreotes[a,1]

[a]Department of Cell Biology, The Johns Hopkins University School of Medicine, Baltimore, MD 21205; and [b]Department of Electrical and Computer Engineering, The Johns Hopkins University, Baltimore, MD 21218

Contributed by Peter N. Devreotes, May 21, 2015 (sent for review December 20, 2014; reviewed by Denise J. Montell)

**Asymmetric protein localization is essential for cell polarity and migration. We report a novel protein, Callipygian (CynA), which localizes to the lagging edge before other proteins and becomes more tightly restricted as cells polarize; additionally, it accumulates in the cleavage furrow during cytokinesis. CynA protein that is tightly localized, or "clustered," to the cell rear is immobile, but when polarity is disrupted, it disperses throughout the membrane and responds to uniform chemoattractant stimulation by transiently localizing to the cytosol. These behaviors require a pleckstrin homology-domain membrane tether and a WD40 clustering domain, which can also direct other membrane proteins to the back. Fragments of CynA lacking the pleckstrin homology domain, which are normally found in the cytosol, localize to the lagging edge membrane when coexpressed with full-length protein, showing that CynA clustering is mediated by oligomerization. Cells lacking CynA have aberrant lateral protrusions, altered leading-edge morphology, and decreased directional persistence, whereas those overexpressing the protein display exaggerated features of polarity. Consistently, actin polymerization is inhibited at sites of CynA accumulation, thereby restricting protrusions to the opposite edge. We suggest that the mutual antagonism between CynA and regions of responsiveness creates a positive feedback loop that restricts CynA to the rear and contributes to the establishment of the cell axis.**

chemotaxis | polarity | asymmetry | *Dictyostelium* | protein localization

The directional migration of polarized cells toward a chemical gradient plays a critical role in many normal biological processes during development and homeostasis. In addition, polarity and chemotaxis are involved in the pathogenesis of many diseases, including asthma, atherosclerosis, and cancer metastasis. Despite its significance, investigators have only begun to fully appreciate the mechanisms of polarity and directed migration.

Many of the signaling molecules that mediate these events are localized or activated specifically at the leading or, more rarely, lagging edge of migrating cells (reviewed in ref. 1). Events that occur at the leading edge include the activation of Ras, TORC2, and AKT/PKB proteins, accumulation of phosphatidylinositol (3,4,5)-trisphosphate ($PIP_3$), recruitment of several cytoskeletal proteins, and actin polymerization; proteins that accumulate at the lagging edge include the lipid phosphatase and tensin homolog deleted on chromosome 10 (PTEN) and Myosin II. Furthermore, these leading- and lagging-edge proteins respond to uniformly applied chemoattractant by transiently relocalizing onto or off of the membrane, respectively. In polarized cells, the asymmetric localization patterns are accentuated and maintained even in the absence of a chemoattractant gradient. Many of these asymmetries are conserved in migratory cells, such as *Dictyostelium discoideum*, mammalian leukocytes, fibroblasts, and axonal growth cones (2–6). In addition, these signaling molecules display characteristic localization patterns that are important for the regulation of other cellular behaviors, such as cytokinesis and phagocytosis, as well as in nonmigratory cells, such as epithelia (7–13).

*D. discoideum* is an excellent model system for studying directional migration because of its genetic accessibility and the nature of its life cycle. Growing *Dictyostelium* cells spontaneously extend transient protrusions in alternating directions, which results in frequent directional changes and poor chemotaxis (14). Upon starvation, the cells differentiate, undergoing a program of gene-expression changes that lead to an increased sensitivity to the chemoattractant cAMP. In addition, differentiation causes cells to elongate, have a differential sensitivity to cAMP along their axis, and extend protrusions preferentially at the front, resulting in improved chemotactic ability (15).

Because many molecules involved in polarity and chemotaxis are localized to the front or back of cells, we designed a screen using *Dictyostelium* to identify novel regulators based on the spatial distributions of GFP-tagged proteins in migrating cells. This approach circumvents the pitfalls of traditional loss-of-function screens for defects in chemotaxis: some regulatory components may be essential for cytokinesis or phagocytosis, resulting in lethal mutations; other important components may be redundant, their loss causing only a partial phenotype (reviewed in ref. 1). Using our localization-based technique, we found a previously unidentified protein at the lagging edge that appears to be part of a positive feedback loop that brings about polarity by acting at the cell rear.

## Results

**Callipygian Localizes to the Rear of Migrating *Dictyostelium* Cells.** Because of their role in $PIP_3$ signaling, pleckstrin homology (PH) domain-containing proteins are likely candidates for asymmetric localization and regulation of chemotaxis. However, PH domains have widely varied binding specificities, and there are more than

### Significance

**Though the asymmetric distribution of proteins is a crucial first step in establishing polarity and guiding cell migration, the molecular mechanisms regulating many of these localizations are unknown. Our study reports on the novel protein Callipygian (CynA), which localizes to the rear of cells during symmetry breaking, thereby promoting polarity and increasing migration efficiency. Our data indicate that CynA localization is mediated by two distinct mechanisms, which may be important for segregating proteins in other polarized cell types including epithelial cells, neurons, and immune cells. Thus, our findings have implications for tissue formation during embryonic development, the migration of immune cells during wound healing and infection, and the aberrant migrations associated with arthritis, asthma, atherosclerosis, cancer metastasis, and other diseases.**

Author contributions: K.F.S. and P.N.D. designed research; K.F.S. performed research; K.F.S., J.B., and P.A.I. contributed new reagents/analytic tools; K.F.S., P.A.I., and P.N.D. analyzed data; and K.F.S., P.A.I., and P.N.D. wrote the paper.

Reviewers included: D.J.M., University of California, Santa Barbara.

The authors declare no conflict of interest.

[1]To whom correspondence should be addressed. Email: pnd@jhmi.edu.

This article contains supporting information online at www.pnas.org/lookup/suppl/doi:10.1073/pnas.1509098112/-/DCSupplemental.

100 PH domain-containing proteins in *Dictyostelium* (16, 17). We focused on a group of 23 *Dictyostelium* PH domain-containing proteins that were predicted to bind specifically to $PIP_3$ using an algorithm that was generated by comparing the sequences of $PIP_3$-responsive and $PIP_3$-nonresponsive domains (18). This subset of PH domain-containing proteins, as well as several random cDNAs, were tagged with GFP, expressed in *Dictyostelium* cells, and assessed for intracellular localization during migration. Unexpectedly, one of the PH domain-containing proteins, PH21, was identified at the lagging edge. We designated it Callipygian (CynA) (DictyBase gene ID DDB_G0284337).

We further characterized the localization of CynA. Consistent with the original observation that CynA-GFP localized to the rear of randomly migrating cells, this protein was found at the lagging edge of differentiated cells migrating in a gradient of chemoattractant (Fig. 1*A* and Movie S1). Furthermore, CynA-GFP was excluded from sites of accumulation of the $PIP_3$ biosensor, $PH_{CRAC}$-RFP, a well-defined leading edge marker, in differentiated cells that were randomly migrating or uniformly stimulated with cAMP (Fig. 1 *B* and *C*) (19). Additionally, CynA-GFP and mCherry-Myosin II, a known lagging-edge protein, both localized to the rear of migrating cells (Fig. 1*D*) (20). Consistent with other proteins found at the lagging edge, CynA-GFP strongly accumulated at the cleavage furrow during both early and late stages of cytokinesis (Fig. 1*E*) (9, 20–23).

To determine whether other lagging-edge proteins are required for the localization of CynA, we expressed CynA-GFP in both *pten*$^-$ and *myo II*$^-$ cells, induced differentiation, and assessed the CynA-GFP distribution pattern during random migration and chemotaxis. In both mutant cell lines, CynA-GFP localized to the rear of migrating cells as it did in wild-type cells, suggesting that CynA localization does not require either PTEN or Myosin II (Fig. 1*F*). However, in addition to its localization at the lagging edge, CynA-GFP showed several other distribution patterns in *pten*$^-$ cells; for example, CynA-GFP was often found on convex regions of curvature on the top surface rather than on the lateral surface, as in wild-type or most *pten*$^-$ cells, or in membrane-adjacent cytosolic patches (Fig. S1*A*). This finding suggests that CynA-GFP is targeted less efficiently to the lagging edge, or its localization at the rear is less stable, in *pten*$^-$ cells, likely because of the dynamic morphological changes observed in this mutant strain (24).

CynA-GFP appeared to be more tightly limited to the cell rear than other lagging-edge proteins. Before differentiation, Myosin II, PakA, and PTEN are found uniformly around the cell periphery, with the exception of protrusions, and gradually become restricted to the lagging edge as differentiation progresses and cells polarize (20, 23, 24). In contrast, CynA-GFP was found only at the back of randomly migrating, undifferentiated cells, whereas other back markers were still uniformly localized (Fig. 1 *G* and *H* and Movie S2). This result suggests that the spatial targeting of CynA occurs before the polarization of other chemotactic signaling molecules, consistent with the observation that CynA does not require either PTEN or Myosin II to localize to the rear. In ∼80% of growing cells, the back-most region, where the accumulation of CynA-GFP was strongest, actually appeared to be depleted of mCherry-Myosin II relative to other portions of the cortex (Fig. S1*B*).

**CynA Localization Is Regulated by Chemoattractant Stimulation.** We next assessed the dynamics of CynA localization. To test whether CynA localization is responsive to chemoattractant, we expressed CynA-GFP in wild-type cells, allowed the cells to differentiate to induce chemotactic sensitivity, and stimulated them uniformly with 1 μM cAMP. In the vast majority of cells, CynA-GFP was strongly restricted to the lagging edge, and this distribution was largely unchanged upon the addition of cAMP (Fig. 2*A*). To test whether the polarized shape of differentiated cells influences the response of CynA to chemoattractant, we disrupted the actin cytoskeleton by

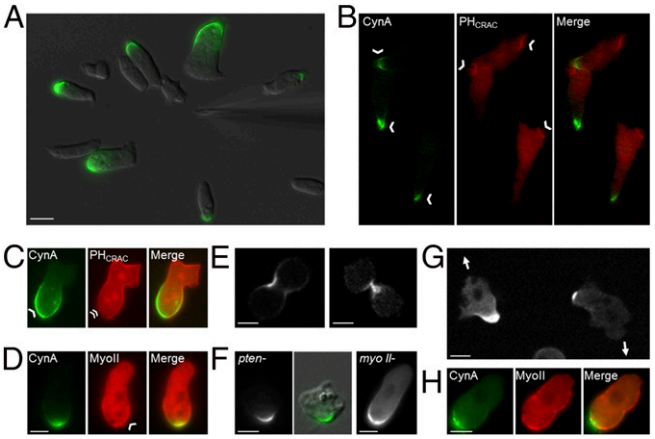


**Fig. 1.** CynA is a novel protein that localizes asymmetrically independently of other lagging edge proteins. (*A*) Differentiated *Dictyostelium* cells expressing CynA-GFP were imaged by time-lapse fluorescence microscopy while migrating toward a micropipette filled with the chemoattractant cAMP. (*B* and *C*) Differentiated cells coexpressing CynA-GFP and $PH_{CRAC}$-RFP were imaged during aggregation (*B*) or 5 s after uniform stimulation with 1 μM cAMP (*C*). Arrowheads indicate sites of protein accumulation; the double arrowhead indicates an absence of $PH_{CRAC}$-RFP at the site of CynA-GFP localization. (*D*) Differentiated cells coexpressing CynA-GFP and mCherry-Myosin II were imaged. An arrowhead indicates mCherry-Myosin II accumulation. (*E*) Wild-type cells expressing CynA-GFP were imaged during early (*Left*) and late (*Right*) stages of cytokinesis. (*F*) Differentiated *pten*$^-$ (*Left*) and *myosin II*$^-$ (*Right*) cells expressing CynA-GFP were imaged during random migration. The center panel shows a merge of the DIC and GFP fluorescence images for the *pten*$^-$ cell to illustrate the localization of CynA-GFP relative to the cell morphology. (*G*) Undifferentiated wild-type cells expressing CynA-GFP were imaged during random migration. Arrows indicate the direction of migration for each cell. (*H*) Undifferentiated cells coexpressing CynA-GFP and mCherry-Myosin II were imaged. The direction of migration was toward the top of the panels unless noted. (Scale bars, 5 μm.)

treating with 1 μM Latrunculin A, which caused the cells to round up. This morphological change resulted in the dispersal of CynA-GFP from the lagging edge to the entire cell periphery (Fig. 2*B*). In Latrunculin-treated cells that were uniformly stimulated, CynA-GFP translocated into the cytosol within 10 s and began to slowly return to the membrane within 30 s, although about half of the cells show less than 50% recovery of the CynA-GFP membrane signal (Fig. 2 *C* and *D* and Movie S3). This translocation also occurred in the 10% of cells that were intrinsically rounded even in the absence of Latrunculin (Fig. S2 *A* and *B*). With slightly faster kinetics, $PH_{CRAC}$-RFP transiently translocated onto the plasma membrane (Fig. S2 *C* and *D*). These transient redistributions in response to global stimulation are characteristic of other known "front" and "back" proteins (1, 24–30). Taken together, these observations suggest that the accumulation of CynA at the lagging edge is stabilized in polarized cells, preventing the protein from relocalizing in response to chemoattractant.

Other conditions that altered cell morphology also delocalized CynA-GFP. First, in the ∼10% of cells that did not elongate strongly during differentiation, CynA-GFP was more dispersed around the cell periphery than in highly elongated cells (Fig. S2*A*). Second, cells exposed to excessive light gradually rounded up and the distribution of CynA-GFP at the membrane became uniform (Fig. S2*E*). Third, growing cells were occasionally quiescent, with fewer productive protrusions and a rounder morphology than their actively migrating counterparts, because of day-to-day variations; the distribution of CynA-GFP at the membrane was more dispersed in these cells (Fig. S2*F*). Fourth, when randomly migrating growing cells reversed their direction, CynA-GFP became diffuse before relocalizing to the new rear within roughly 30 s (Fig. S2*G*). Interestingly, a predominant CynA-GFP

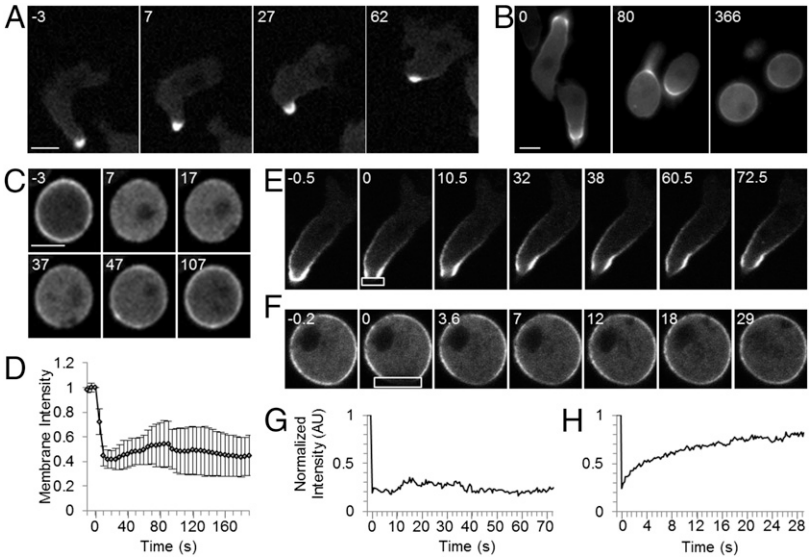


**Fig. 2.** CynA accumulation at the cell periphery is stabilized by polarity. (*A*) Differentiated cells expressing CynA-GFP were stimulated uniformly with 1 μM cAMP and imaged by fluorescence microscopy at 5-s intervals. Time (s) after the addition of cAMP is indicated. (*B*) Differentiated cells expressing CynA-GFP were treated with 0.5 μM Latrunculin A and imaged every 3 s. Time (s) after the addition of Latrunculin A is indicated. (*C* and *D*) Differentiated cells expressing CynA-GFP were treated with 1 μM Latrunculin A, stimulated with 1 μM cAMP and imaged every 5 s (*C*). Time (s) after the addition of cAMP is indicated. The mean membrane intensity was calculated as described (see *SI Materials and Methods*) (*D*). Shown is the mean ± SD ($n$ = 38 cells from eight movies). (*E–H*) Differentiated cells expressing CynA-GFP were assessed by FRAP with (*F* and *H*) or without (*E* and *G*) 1 μM Latrunculin A treatment. Time (s) after photobleaching the region indicated by the box is shown. For the cells shown in *E* and *F*, the normalized fluorescence intensity was measured as described (*SI Materials and Methods*) and plotted (*G* and *H*, respectively). (Scale bars, 5 μm.)

signal remained on the membrane throughout this process. Taken together, these observations suggest that asymmetric cell shape regulates the intracellular distribution of CynA.

We next tested the effect of cell morphology on CynA protein mobility using fluorescence recovery after photobleaching (FRAP). In highly motile elongated cells, the fluorescent signal that was lost after CynA-GFP was photobleached at the lagging edge did not recover over the course of 72 s (Fig. 2 *E* and *G* and Movie S4). Thus, the diffusion of CynA in polarized cells occurs more slowly than would be expected for a typical membrane protein. However, in cells pretreated with Latrunculin A, roughly 80% of the CynA-GFP fluorescence recovered from cytosolic pools, because the bleached region filled in uniformly. The recovery was biphasic, with 20% recovering with a half-time of 1.5 s, and 80% recovering with a half-time of 40 s (Fig. 2 *F* and *H* and Movie S4). Furthermore, undifferentiated cells, which are highly photosensitive, often acquired a rounded morphology because of light damage during the course of FRAP analysis, causing CynA-GFP to spread more uniformly around the cell periphery. In these cells, the fluorescence recovered similarly to that of Latrunculin-treated cells (10% recovering with a half-time of 100 ms, and 90% recovering with a half-time of 20 s). Taken together, these results suggest that membrane-bound CynA can exchange rapidly with cytosolic pools, but this exchange no longer occurs as CynA becomes stably localized to the cell rear in polarized cells.

**Localization of CynA to the Lagging Edge Depends on a WD40 Clustering Domain and a Membrane Tether.** We further characterized the domain composition of CynA. In addition to its N-terminal PH domain (amino acids 10–144), CynA contains a putative WD40 domain and a long C-terminal extension (Fig. 3*A*). The WDSP WD40-repeat protein structure predictor found a full seven-bladed propeller in the CynA sequence (amino acids 278–616) (31). A seven-bladed propeller structure was also supported by a model of CynA generated by the threading software RaptorX, which found seven adjacent four-strand–containing β-sheets, although these sheets were separated into two distinct clusters in this model (32). Although CynA lacks sequence homology to proteins in higher eukaryotes, it may have functional homologs because several mammalian proteins share a similar domain composition. For example, the Rho GEF ARHGEF10 and several BEACH domain family proteins, including neurobeachin (NBEA), lipopolysaccharide-responsive, beige-like anchor protein (LRBA), lysosomal trafficking regulator (LYST), and neutral sphingomyelinase activation-associated factor (NSMAF), contain both WD40 and PH domains (33).

The PH domain of CynA was predicted to bind $PIP_3$; however, CynA-GFP in cell lysates bound to many of a series of lipids spotted on hydrophobic membranes (Fig. S3*A*), with a slight preference for $PI(3,4)P_2$ and no preference for $PIP_3$. This finding suggests that binding of a specific lipid is not the key regulator of CynA localization. Furthermore, the localization of CynA-GFP was unaffected by the addition of the PI3K inhibitor LY294002, which has been shown to greatly reduce $PIP_3$ levels in vivo (Fig. S3*B*) (34). This finding is consistent with the observation that CynA-GFP and $PIP_3$ biosensors were not colocalized (Fig. 1 *B* and *C*).

To determine which region of the CynA protein controls localization to the lagging edge, we generated a series of GFP-tagged C- and N-terminal truncation constructs and expressed them in undifferentiated cells and in polarized cells undergoing chemotaxis (Fig. 3*A*). $CynA_{1–204}$ localized mostly to the cytosol, but appeared weakly on the plasma membrane, with enrichment at the rear, in a small percentage of actively migrating cells (Fig. 3*B*). $CynA_{1–325}$ displayed greatly increased localization to the lagging edge, but compared with the full-length protein there was an increased cytoplasmic pool of fluorescent protein, fewer cells showed strong membrane localization after treatment with Latrunculin A, strong accumulation at the back was not apparent in less motile cells compared with chemotaxing cells, and the signal at the back could recover rapidly after photobleaching (Fig. 3 *B–D* and Fig. S3 *C* and *D*). $CynA_{1–574}$, like the full-length protein, was strongly bound to the membrane, even after Latrunculin A treatment, and tightly accumulated at the rear even in relatively unpolarized cells (Fig. 3 *B* and *C* and Fig. S3*C*). Longer

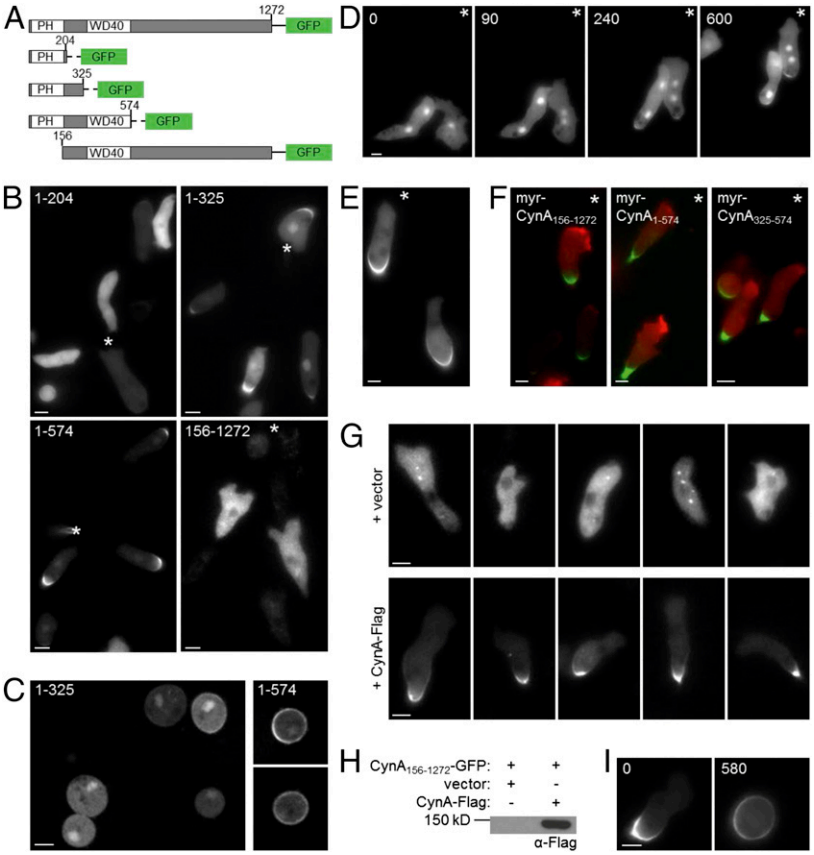


**Fig. 3.** CynA localization is specified by its PH and WD40 domains. (*A*) A schematic representation of the GFP-tagged CynA protein (*Top*) and a series of GFP-tagged CynA truncation constructs. (*B*) Differentiated cells expressing the indicated GFP-tagged truncation constructs, depicted in *A*, were imaged by time-lapse fluorescence microscopy while migrating toward a micropipette filled with cAMP. Asterisks indicate the position of the micropipette. (*C*) Differentiated cells expressing the indicated GFP-tagged truncations of CynA were treated with 1 μM Latrunculin A and imaged. (*D*) Differentiated cells expressing $CynA_{1–325}$-GFP were imaged at 30-s intervals while migrating toward a micropipette filled with cAMP. Time (s) after the cAMP gradient was established is indicated. Asterisks indicate the position of the micropipette. (*E*) Differentiated cells expressing $CynA_{1–204+1–204}$-GFP were imaged while migrating toward a micropipette filled with cAMP, indicated by an asterisk. (*F*) Differentiated cells coexpressing the indicated myristoylated, GFP-tagged truncations of CynA and $LimE_{\Delta coil}$-RFP were imaged while migrating toward a micropipette filled with cAMP. The images shown are a merge of the RFP and GFP channels. The asterisk marks the position of the micropipette. (*G–I*) Differentiated cells coexpressing $CynA_{156–1272}$-GFP and either a vector control or CynA-Flag, as indicated, were imaged while migrating toward a micropipette filled with cAMP (toward the top of each panel). The images shown were acquired using the GFP channel (*G*). Western blot analysis indicates the expression of CynA-Flag in the cell population (*H*). Coexpressing cells were treated with 5 μM Latrunculin A after two frames and imaged using GFP illumination every 10 s. Time (s) after the addition of Latrunculin A is indicated (*I*). (Scale bars, 5 μm.)

N-terminal fragments of CynA were also enriched at the lagging edge, although the extent of membrane accumulation varied between the different truncated proteins. $CynA_{156–1272}$ and other N-terminal truncations localized to the cytosol, although protein expression was low (Fig. 3*B*). The results of the truncation analyses suggest that the PH domain of CynA is required for membrane binding and that the N-terminal 574 amino acids are sufficient for tight accumulation at the lagging edge.

We next wanted to test whether the PH domain was also sufficient for membrane binding. The PH domain alone, $CynA_{1–204}$, localized weakly to the plasma membrane (Fig. 3*B*); therefore, we artificially fused two copies of the PH domain in a single construct to increase membrane affinity. This GFP-tagged tandem PH domain protein localized strongly to the rear of highly motile elongated cells but localized more globally to the plasma membrane in undifferentiated cells, similarly to $CynA_{1–325}$ (Fig. 3*E*). Furthermore, when cells were pretreated with Latrunculin A and stimulated uniformly, the tandem PH domain protein transiently relocalized from the membrane to the cytosol (Movie S5). This finding suggests that the PH domain is sufficient to bind to and sense the properties of the plasma membrane that determine the front versus back state.

To test whether the membrane binding and strong back-targeting functions of CynA are separable, we fused $CynA_{156–1272}$-GFP, which is located in the cytosol, to the myristoylated N-terminal portion (amino acids 1–128) of PKBR1, which is distributed uniformly on the membrane (35). Remarkably, this chimeric protein localized tightly to the lagging edge, essentially identically to the full-length CynA-GFP (Fig. 3*F* and Fig. S3*E*). Furthermore, regions containing just the WD40 region of CynA ($CynA_{156–574}$ and $CynA_{325–574}$), which lack membrane localization on their own, were sufficient to localize strongly to the plasma membrane at the cell rear when fused to the exogenous myristoylation motif (Fig. 3*F* and Fig. S3 *E* and *F*). The data shown in Fig. 3 *E* and *F* suggest that the localization of CynA is regulated by two distinct mechanisms. First, the PH domain controls binding to the membrane and senses external cues. Second, a "clustering" motif, located between amino acids 325 and 574, causes the accumulation of membrane-bound CynA at the rear of cells; this region corresponds to the putative WD40 domain.

Several pieces of evidence suggested that the WD40 region of CynA may be mediating oligomerization events, including the increased membrane binding observed for the dimerized PH domain, the tightly clustered localization of the WD40-containing

region, which correlates with reduced protein mobility as observed by FRAP, and the observation that a smaller WD40 region, $CynA_{325–574}$, localized to small intracellular puncta (Fig. S3*F*). To test whether CynA can self-oligomerize, we coexpressed a GFP-tagged, cytosol-localized portion of CynA, $CynA_{156–1272}$-GFP, with either empty vector or a full-length Flag-tagged CynA protein (Fig. 3 *G* and *H*). Coexpression with empty vector resulted in a cytosolic and occasionally (about 20% of cells) punctate GFP signal, as observed for $CynA_{156–1272}$-GFP alone. However, when this protein was coexpressed with full-length CynA-Flag, the GFP-tagged protein was detected at the lagging edge of 95% of cells that had a detectable GFP signal (Fig. 3 *G* and *H*). $CynA_{156–574}$-GFP also localized to the lagging edge when coexpressed with CynA-Flag in a small percentage of cells (~5%) (Fig. S3*G*). This finding indicates that full-length CynA-Flag could bind to and mediate the proper lagging edge membrane localization of the portion of CynA that includes the WD40 domain. Treatment with Latrunculin A led to uniform localization but did not reverse the membrane association of $CynA_{156–1272}$-GFP in these coexpressing cells, indicating that the actin cytoskeleton and polarity are not required for CynA oligomerization (Fig. 3*I*).

**CynA Mediates Cell Morphology and Migration.** To study the function of CynA, we generated several independent null strains using homologous recombination (Fig. S4*A*). The resulting mutants were plated as a monolayer on nonnutrient agar and assessed for differentiation and chemotaxis. Under these conditions, wild-type cells differentiated and formed streams of migrating cells by the 5-h stage (36). The *cynA*⁻ cells also formed streams and aggregated, but this process was delayed by about 2 h for two independently disrupted cell lines (Fig. 4*A*). This delay in early differentiation was reversed by expressing CynA-GFP in the *cynA*⁻ cells, suggesting that the GFP-tagged protein is functional (Fig. 4*A*). Furthermore, exogenous expression of CynA-GFP in wild-type cells caused streaming and aggregation behaviors to be accelerated by about 2 h (Fig. 4*A*).

To further characterize the developmental delay of *cynA*⁻ cells, we imaged cells that were washed off of nonnutrient agar plates at various time points throughout differentiation. Cells expressing CynA-GFP became elongated at earlier time points in differentiation than the *cynA*⁻ cells (Fig. 4 *B* and *C* and Fig. S4*B*). In fact, the difference in morphology across cell types is even more pronounced than the data suggest, because many of the CynA-GFP–expressing cells aggregated during imaging and could not be included in the analyses. Additionally, 50% of *cynA*⁻ cells retained protrusions around their lateral edges even after becoming elongated (Fig. 4*B*). Endogenous cAR1 protein, a well-characterized marker for cell differentiation, was up-regulated on a similar timescale for wild-type and *cynA*⁻ cells, as well as for cells exogenously expressing CynA-GFP (Fig. 4*D*) (37, 38). Interestingly, endogenous cAR1 levels began to decline at earlier time points in cells expressing CynA-GFP compared with wild-type or *cynA*⁻ strains. The precocious down-regulation of cAR1 may be caused by the earlier aggregation of these cells because it was not observed when cells were differentiated in suspension.

The differences in morphology observed for *cynA*⁻ cells also translated to defects in random migration. Tracks of *cynA*⁻ cell motility were shorter and had a jagged trajectory compared with wild-type, whereas tracks for cells overexpressing CynA-GFP were longer and straighter on average (Fig. 4*E*). Furthermore, *cynA*⁻ cells moved with decreased directional persistence and similar speeds compared with wild-type cells throughout differentiation. Conversely, cells expressing CynA-GFP migrated with increased persistence and became faster at an earlier time point. After about 3 h of differentiation, cells expressing CynA-GFP began to aggregate immediately upon plating for imaging; the added component of gradient sensing and chemotaxis appeared

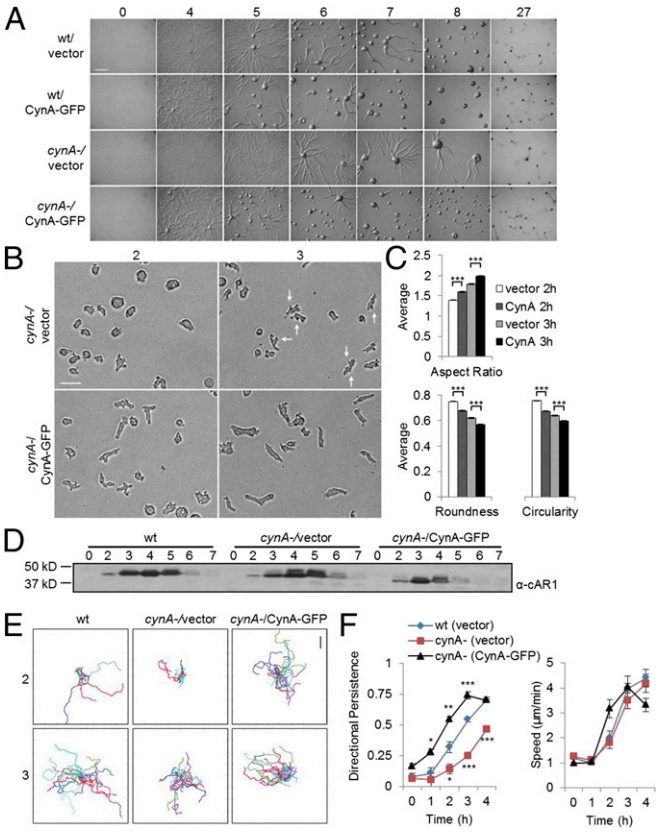


**Fig. 4.** CynA affects aggregation and polarity during early differentiation. (*A*) Undifferentiated wild-type or *cynA*⁻ cells expressing either CynA-GFP or a vector control were plated onto nonnutrient agar at a density of $5 \times 10^5$ cells/cm$^2$ and imaged as they proceeded through differentiation. Time (h) of starvation is indicated. (Scale bar, 1 mm.) (*B*–*D*) Cells were prepared on sets of nonnutrient agar plates as in *A* and collected for further analysis over the course of differentiation. A fraction of the cells was imaged during random migration for 30 min at 30-s intervals by multipoint time-lapse microscopy (*B*); cells were also lysed and analyzed by Western blotting, using antibodies against the endogenous cAR1 protein (*D*). Time (h) of differentiation is indicated. The images shown in *B* were acquired after 30 min of imaging and include arrows to indicate some of the lateral protrusions. (Scale bar, 25 μm.) The morphology of *cynA*⁻ cells, expressing either the KF2 vector control or CynA-GFP and imaged after either 2 or 3 h of differentiation as in *B*, were quantified using ImageJ (*C*). Each bar on the graph represents the mean ± SEM ($n$ > 1,300 cells, taken from three separate experiments per sample). ***$P$ < 0.001. (*E* and *F*) Cells were differentiated on nonnutrient agar and imaged during random migration as in *B*, and cell centroids were tracked manually to generate trajectories (*E*) and measure motility parameters (*F*) as described in *SI Materials and Methods*. Tracks in *E* show 25–35 cells per sample. (Scale bar, 100 μm.) Each data point in the graphs in *F* represent the average of the means ± SEM ($n$ = 4 movies, with 25 cells each, per sample). *$P$ < 0.05, **$P$ < 0.02, ***$P$ < 0.01 (all comparisons to wild-type with a Bonferroni correction).

to decrease cell speed, resulting in shorter tracks, while further increasing directional persistence (Fig. 4 *E* and *F*).

**CynA Affects the Morphology and Behavior of Cells in Response to Chemoattractant Gradients.** Using a micropipette assay to test chemotaxis, *cynA*⁻ cells sensed the gradient of chemoattractant and migrated toward the cAMP source (Fig. 5*A* and Movies S6 and S7). We observed similar behavior in *myo II*⁻ cells, which elongated and aligned in the direction of a chemoattractant source despite their known polarity defects (Fig. 1*F*) (39–43). Although *cynA*⁻ cells could chemotax with wild-type–like motility speeds (3.70 ± 0.11 μm/min for *cynA*⁻ vs. 3.45 ± 0.19 μm/min for

wild-type; $P = 0.25$; data are the mean ± SEM, $n = 80$ or 180 cells for wild-type or *cynA*⁻, respectively), these cells showed slight decreases in directional persistence (0.48 ± 0.02 for *cynA*⁻ vs. 0.65 ± 0.03 for wild-type; $P < 0.01$), chemotactic index (0.35 ± 0.02 for *cynA*⁻ vs. 0.53 ± 0.03 for wild-type; $P < 0.01$) and chemotactic speed (1.17 ± 0.08 μm/min for *cynA*⁻ vs. 1.91 ± 0.18 μm/min for wild-type; $P < 0.01$). Expression of CynA-GFP, but not an empty vector, in the *cynA*⁻ cells was able to reverse these defects in directional persistence (0.51 ± 0.02 for CynA-GFP vs. 0.42 ± 0.02 for vector; $P < 0.01$; data are the mean ± SEM, $n = 152$ or 183 cells for CynA-GFP or vector expression, respectively), chemotactic index (0.37 ± 0.03 for CynA-GFP vs. 0.30 ± 0.02 for vector; $P = 0.02$), and chemotactic speed (1.89 ± 0.19 μm/min for CynA-GFP vs. 1.11± 0.10 μm/min for vector; $P < 0.01$). As with cells that were differentiated on nonnutrient agar, the *cynA*⁻ cells appeared to have altered morphologies compared with wild-type controls during chemotaxis. Although they were still elongated, *cynA*⁻ cells frequently had lateral pseudopodia that were not observed in wild-type cells (Fig. 5*A*). These aberrant protrusions could potentially explain the decreased speed and persistence observed during chemotaxis. Despite these defects, PTEN, Myosin II, and $PIP_3$ markers were still able to localize asymmetrically during late stages of differentiation in *cynA*⁻ cells (Fig. S5*A*).

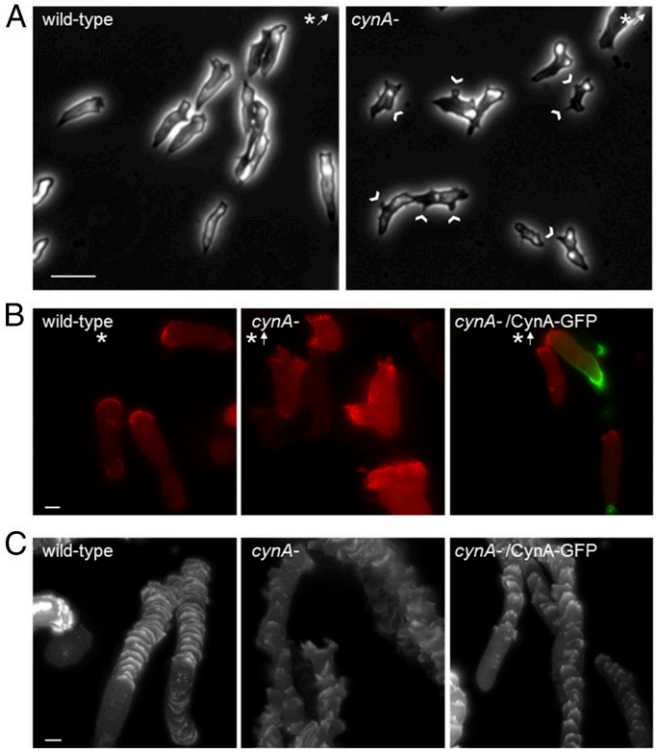


**Fig. 5.** Disruption of CynA leads to an increase in lateral protrusions and an altered leading edge morphology. (*A*) Differentiated wild-type and *cynA*⁻ cells were imaged by time-lapse microscopy for 30 min at 30-s intervals while migrating toward a micropipette filled with cAMP. Images are shown for the last frame. Asterisks indicate the position of the micropipette; arrows indicate that the micropipette was placed outside of the frame shown. Arrowheads indicate lateral protrusions. (Scale bar, 20 μm.) (*B* and *C*) Differentiated wild-type and *cynA*⁻ cells coexpressing $LimE_{\Delta coil}$-RFP and either CynA-GFP or empty vector were imaged by fluorescence microscopy at 30-s intervals while chemotaxing toward a micropipette filled with cAMP (*B*). The images shown in *B* are a merge of the GFP and RFP channels. Tracks of the RFP fluorescence intensities for the cells shown in *B* were generated using ImageJ, such that each pixel shown in the overlaid image corresponds to the maximum pixel intensity for that location over the course of the movie (*C*). The first 5 min of each movie, during which cells were turning to orient toward the cAMP gradient, were excluded from analysis in *C* for simplification. Asterisks indicate the position of the micropipette; arrows indicate that the micropipette was placed outside of the frame shown. (Scale bars, 5 μm.)

We next tested the effect of CynA-GFP overexpression in cells responding to shifting chemoattractant gradients. These cells were more elongated and had fewer lateral protrusions than control cells. Following repositioning of the micropipette, the control cells extended protrusions toward the new chemoattractant source, whereas the CynA-GFP–expressing cells maintained their existing fronts and turned (Fig. S5 *B* and *C*). Furthermore, CynA-GFP was consistently localized to the lagging edge, even when the micropipette was positioned directly behind the cells (Fig. S5*C*).

To better observe the morphology defects of the *cynA*⁻ strain, we expressed $LimE_{\Delta coil}$-RFP, a marker for newly polymerized actin, and assessed chemotaxis (44). Consistent with previous results, *cynA*⁻ cells displayed a broader distribution of $LimE_{\Delta coil}$-RFP at the leading edge than wild-type cells or *cynA*⁻ cells expressing CynA-GFP (Fig. 5 *B* and *C* and Movies S8 and S9). Furthermore, *cynA*⁻ cells, but not those expressing CynA-GFP, showed the accumulation of $LimE_{\Delta coil}$-RFP at multiple additional sites along the cell perimeter, indicating excessive pseudopod formation (Fig. 5 *B* and *C* and Movies S8 and S9). Expression of $LimE_{\Delta coil}$-RFP also highlighted differences across cell lines in the shape of pseudopodia. Whereas the edges of protrusions in *cynA*⁻ cells were jagged and dynamic, moving rapidly from side to side, those in wild-type cells had smooth edges and extended evenly (Fig. 5 *B* and *C* and Movies S8 and S9).

**CynA Spatially Restricts Actin Polymerization.** We next compared the localizations of CynA-GFP and $LimE_{\Delta coil}$-RFP. In growing cells, which have reduced polarity but greater spontaneous actin polymerization than differentiated cells, CynA-GFP and $LimE_{\Delta coil}$-RFP had opposing distributions (Fig. 6*A*). This was true even for the most active cells, which extended actin protrusions all around the cell periphery, occasionally resulting in a broader distribution or multiple sites of CynA-GFP accumulation (Fig. 6*B* and Fig. S2*F*). In these cells, an actin protrusion extended near sites of CynA-GFP accumulation about 15% of the time, resulting in the retraction of that protrusion and cell movement in the original direction. Rarely, an actin protrusion broke through the patch of CynA-GFP accumulation; when this occurred, the CynA-GFP cluster dispersed such that the two proteins did not colocalize (Fig. 6*B* and Fig. S2*G*). These protrusions were most often rapidly retracted, but also occasionally resulted in a directional change.

The mutually exclusive localizations of CynA-GFP and $LimE_{\Delta coil}$-RFP, as well as the increase in cortical $LimE_{\Delta coil}$-RFP in *cynA*⁻ cells, suggest an antagonistic relationship between CynA and actin polymerization. We tested this connection by observing the response in globally stimulated cells. Following uniform chemoattractant addition, $LimE_{\Delta coil}$-RFP was recruited to the cortex within 10 s of cAMP stimulation and returned to the cytosol by 20 s (Fig. 6*C* and Movie S10). Interestingly, although the cells were stimulated uniformly, $LimE_{\Delta coil}$-RFP was not recruited to the cortex at the rear of wild-type or CynA-GFP-expressing cells (Fig. 6 *C*–*E* and Movie S10). In cells exogenously expressing CynA-GFP, the patch of cortex without $LimE_{\Delta coil}$-RFP recruitment corresponded to sites of CynA-GFP accumulation (Fig. 6 *C*–*E* and Movie S10). In contrast, $LimE_{\Delta coil}$-RFP was recruited uniformly around the cell periphery, including the back, in *cynA*⁻ cells that were differentiated for equivalent amounts of time (Fig. 6 *C*–*E* and Movie S10). Furthermore, the *cynA*⁻ cells appeared to have a slightly prolonged and elevated actin response compared with cells expressing CynA. Accumulation of CynA-GFP did not prevent the localization of cAR1-RFP to the plasma membrane, indicating that the absence of $LimE_{\Delta coil}$-RFP at these sites was not an imaging artifact (Fig. 6*F*). Together, these results suggest that the presence of CynA

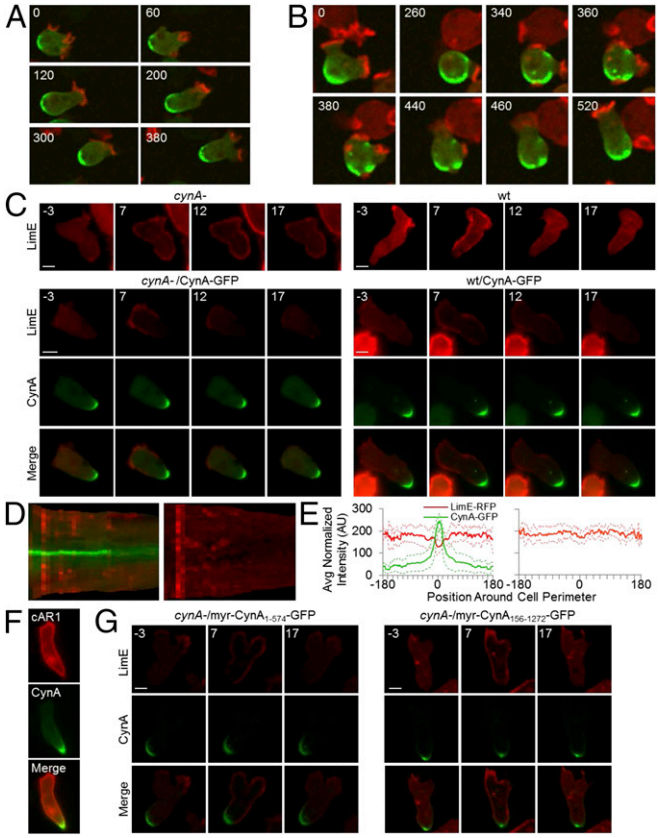


**Fig. 6.** CynA locally inhibits actin polymerization. (*A* and *B*) Undifferentiated *cynA*⁻ cells coexpressing CynA-GFP and $LimE_{\Delta coil}$-RFP were imaged for 10 min at 20-s intervals while migrating. The images shown are a merge of the GFP and RFP channels. Time (s) is indicated. (*C*–*E*) Differentiated wild-type and *cynA*⁻ cells coexpressing $LimE_{\Delta coil}$-RFP and either CynA-GFP or the KF2 vector control were stimulated with 1 μM cAMP and imaged for 2.5 min at 5-s intervals (*C*). Time (s) after the addition of cAMP is indicated. The fluorescence intensities of *cynA*⁻ cells, coexpressing $LimE_{\Delta coil}$-RFP and either CynA-GFP (*Left*) or the KF2 vector control (*Right*), stimulated with cAMP as in *C*, were converted into kymographs (*D*), such that each vertical bar in the kymograph represents the intensities of GFP and RFP (*Left*) or RFP alone (*Right*) along the perimeter of the cell for a given point in time. cAMP was added after the second frame. The fluorescence intensities along the perimeter of *cynA*⁻ cells coexpressing $LimE_{\Delta coil}$-RFP and either CynA-GFP (*Left*) or the KF2 vector control (*Right*), stimulated with cAMP as in *C*, were plotted for the time point corresponding to the maximal chemoattractant response, which occurred 7 s after stimulation (*E*). Solid lines represent the mean ($n \geq 11$ cells), and dotted lines represent the mean ± SD. Before averaging, the fluorescence intensities for each cell were aligned such that 0° corresponds to the morphological back of each cell. In cells expressing CynA-GFP, the $LimE_{\Delta coil}$-RFP intensities of the pixels centered around the cell rear were significantly lower than those at the other regions of the cell boundary when compared by a Student's *t* test (mean ± SEM: 134.16 ± 2.14 at the rear vs. 180.14 ± 0.86 at the nonrear, $P < 0.01$); $LimE_{\Delta coil}$-RFP pixel intensities at the cell rear were also significantly lower in CynA-GFP-expressing cells than in *cynA*⁻ cells (mean ± SEM: 134.16 ± 2.14 for CynA-GFP vs. 151.69 ± 2.39 for *cynA*⁻, $P < 0.01$). (*F*) Differentiated cells coexpressing cAR1-RFP and CynA-GFP were imaged as in *C*. (*G*) Differentiated *cynA*⁻ cells coexpressing $LimE_{\Delta coil}$-RFP and either $myr_{PKBR1}$-$CynA_{1–574}$-GFP or $myr_{PKBR1}$-$CynA_{156–1272}$-GFP were stimulated with 1 μM cAMP and imaged for 2.5 min at 5-s intervals. Time (s) after the addition of cAMP is indicated. (Scale bars, 5 μm.)

locally inhibits actin polymerization in response to cAMP stimulation and during random migration in unstimulated cells. Furthermore, GFP-tagged truncations of CynA that localized to the lagging edge also blocked the actin response in globally stimulated cells. Specifically, fusions of $CynA_{1–574}$-GFP or $CynA_{156–1272}$-GFP to the myristoylation motif of PKBR1 both localized to the lagging edge and restricted actin polymerization, suggesting that the clustering activity of the CynA WD40 domain is sufficient for this inhibition (Fig. 6*G* and Movie S10).

**CynA Clusters Chemoattractant Receptors at the Lagging Edge and Locally Inhibits Their Signaling.** To further explore the relationship between CynA and the response to cAMP stimuli, we fused either full-length CynA-GFP or various truncations to the chemoattractant receptor cAR1, a GPCR with seven transmembrane domains that localizes uniformly throughout the plasma and internal membranes (Fig. 6*F*) (45). Remarkably, each of the resulting cAR1 fusions localized to the cell rear in both growing and differentiated cells (Fig. 7 *A* and *B*). We next coexpressed the cAR1–CynA fusions with $LimE_{\Delta coil}$-RFP in *car1-/3-* cells, so that cAMP receptor activity originated only at sites of CynA-GFP localization, and tested the actin response. Following global stimulation with cAMP, $LimE_{\Delta coil}$-RFP was transiently recruited to the entire cortex, except in regions of cAR1-CynA accumulation (Fig. 7*C* and Movie S11). This finding suggests that clusters of CynA protein or fragments thereof are capable of blocking actin polymerization even when the majority of detectable signaling is initiated in that spot. The recruitment of $LimE_{\Delta coil}$-RFP to the remainder of the cortex suggests that there may be low levels of cAR1–CynA fusion protein around the perimeter of the cell. These proteins would be capable of initiating a response at the front but not concentrated enough for the inhibitory function of CynA. Alternatively, it is possible that activation signals generated by localized receptors can rapidly become global.

## Discussion

**CynA Is a Novel Lagging-Edge Protein with Membrane-Binding and "Clustering" Domains.** Although CynA shares many similarities to other lagging edge proteins, it also has several unique properties. Like CynA, other back proteins translocate transiently into the

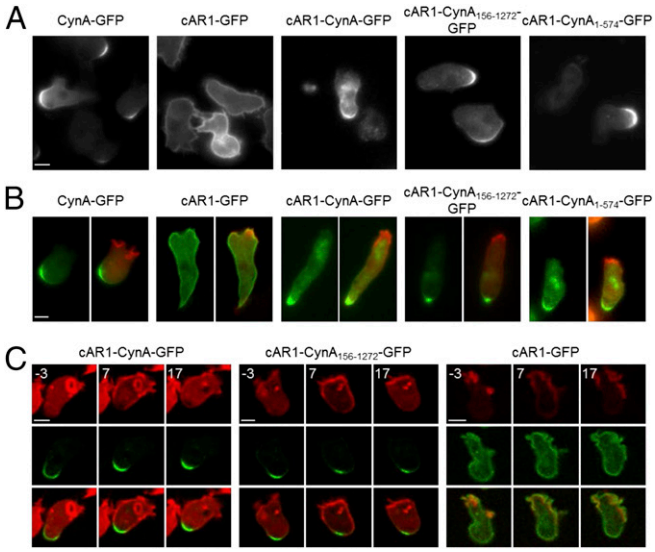


**Fig. 7.** CynA clusters proteins at the lagging edge and locally blocks the chemoattractant response. (*A*) Undifferentiated *car1-/3-* cells expressing the indicated GFP-tagged proteins were imaged by fluorescence microscopy. (*B*) Differentiated *car1-/3-* cells coexpressing $LimE_{\Delta coil}$-RFP and the indicated GFP-tagged proteins were imaged while migrating in the presence of a micropipette filled with cAMP, which was oriented toward the top of each panel. For each cell line, the GFP image is shown alone (*Left*) and merged with the RFP image (*Right*). (*C*) Differentiated *car1-/3-* cells coexpressing $LimE_{\Delta coil}$-RFP and the indicated GFP-tagged proteins were stimulated with 1 μM cAMP and imaged for 2.5 min at 5-s intervals. Time (s) after the addition of cAMP is indicated. (Scale bars, 5 μm.)

cytosol upon chemoattractant stimulation, accumulate in the cleavage furrow during cytokinesis, and have spatial distributions that are tightly coupled to cell polarity. However, CynA localizes asymmetrically in growing cells, whereas the other lagging-edge proteins target to the back only as the cells differentiate (20, 23, 24). Furthermore, CynA accumulation at the rear is more stable and tightly localized than that of other lagging-edge proteins, such as PTEN. In fact, the lagging-edge localization of CynA is strong enough to override the endogenous localizations of other membrane proteins, forcing them to cluster at the back when fused to CynA.

We explored the extrinsic factors that regulate the localization of CynA. First, although the stable asymmetric localization of CynA requires cell polarity or an intact actin cytoskeleton, newly polymerized actin can cause local patches of accumulated CynA to disperse. Second, the localization of CynA does not require PTEN or Myosin II and clustering occurs in growing cells before other proteins become restricted to the lagging edge. Third, the binding site for CynA appears to be up-regulated at the cell rear with differentiation, either by increases in total amount (i.e., via transcriptional regulation) or by increases in local concentrations (i.e., via asymmetric distribution). Finally, although there is speculation that $PI(4,5)P_2$ is important for the localization of PTEN, neither *Dictyostelium* PTEN nor CynA binds to $PI(4,5)P_2$ specifically in vitro (46, 47). In fact, CynA showed a slight preference for $PI(3,4)P_2$ on lipid strips, which indicates either that $PI(3,4)P_2$ is enriched at the lagging edge or that lipid interactions are not important for conferring asymmetric localization.

CynA contains a PH domain required for membrane binding and a WD40 domain that likely regulates oligomerization; these domains mediate binding to the lagging edge via two distinct mechanisms. Like PTEN, the PH domain senses changes in the membrane that cause dissociation both from protrusions and following chemoattractant stimulation, indicating that the PH domain accumulates at the lagging edge by dissociating from the front. In contrast, myristoylated versions of CynA lacking the PH domain remain bound to the membrane during stimulation and thus accumulate at the lagging edge by a different mechanism. The WD40 domain controls this behavior, likely by mediating the formation of higher-order oligomers. It has been reported that high-order oligomerization and membrane-binding motifs artificially target cytosolic proteins to membrane patches, which accumulate at the lagging edge in polarized cells (48–52). Oligomerizing membrane microdomain components also enrich at the rear of polarized neutrophils or T cells (53–57). The WD40 domain enhances the stability and immobility of CynA at the lagging edge, either through oligomerization alone or by interaction with other proteins, as evidenced by the differences between $CynA_{1–574}$ and either $CynA_{1–325}$ or the tandem PH domain, $CynA_{1–204+1–204}$. The formation of large stable complexes with the actomyosin network could explain the dispersal of CynA throughout the membrane upon disruption of the actin cytoskeleton. Moreover, the mechanisms of localization to the rear mediated by the domains of CynA synergize because the WD40 domain requires a membrane anchor for targeting, whereas WD40-mediated oligomerization of the PH domain is expected to enhance its affinity for the membrane.

**CynA Can Be Used as a Tool for Targeting Other Proteins to the Lagging Edge.** The tightly clustered distribution of CynA allows it to serve as a useful tool for targeting other proteins to the lagging edge, opening the way for a multitude of additional studies examining the role of protein localization in migration and many other contexts. We were surprised to find that fusing CynA to several diverse membrane anchors did not affect CynA localization, but rather caused clustering of proteins that are normally distributed uniformly. Thus, we could not test the effects of distributing CynA uniformly throughout the membrane. The fact that CynA recruited cAR1 to the rear allowed us to determine how CynA regulates a localized chemoattractant response. In the future, cAR1–CynA fusions can be used to answer a number of questions related to cAR1 function in migration and adaptation; for example, can cells properly sense a chemoattractant gradient and initiate an appropriate response if receptors are clustered at the cell rear? These and many other potential studies are now possible using CynA as a tool for recruitment to the lagging edge.

**CynA Defines the Axis of Symmetry and Promotes Polarity.** The behavior and localization of CynA suggest a connection with cell polarity. Migrating cells display different degrees of polarity. On one end of the polarity spectrum, a cell extending spontaneous protrusions displays a "transient" polarity. At an intermediate level, cells extending protrusions in the direction of an external cue demonstrate an "induced" polarity. Finally, cells with stable front and back regions, even in the absence of directional cues, exhibit a "persistent" polarity that can be augmented by chemoattractants. Such persistent polarity enhances directionality during migration, allowing cells to chemotax more efficiently in steady gradients, but impairs responsiveness to shifting gradients (15, 58, 59). Undoubtedly, overlapping networks of components are involved in these various events. Our observations indicate that clustered CynA promotes a shift toward the persistent end of the polarity spectrum.

Furthermore, our results suggest that CynA promotes polarity by regulating the localization of actin polymerization and therefore protrusions. Briefly, we found that overexpression of CynA decreases the ability of the lateral or lagging edges of cells to form new extensions toward a source of cAMP. Furthermore, *cynA*$^-$ cells display multiple spontaneous protrusions along the lateral edges, and actin polymerization almost never occurs near sites of CynA accumulation, either spontaneously or in response to a global stimulus, even if receptor-mediated signaling is initiated by receptors clustered at these regions. Experiments using truncated forms of CynA that lack either the N terminus or C terminus of the protein suggest that the clustering domain, $CynA_{156–574}$, is sufficient for these inhibitions of actin polymerization. Of course, CynA may not inhibit actin polymerization directly, but may potentially alter the mechanical properties of the cytoskeleton or act as a negative regulator of signaling events. Because CynA impacts the leading edge morphology, it may regulate a global inhibitory mechanism; alternatively, low levels of CynA protein at the cell front may locally fine-tune the cytoskeletal dynamics.

Combined, these results suggest that the asymmetric localization of CynA is an early step in symmetry breaking and helps establish the axis of polarity. When exogenous CynA-GFP is expressed in growing cells, it accumulates in a patch on the membrane, locally repressing pseudopod formation. This contributes to the creation of a functional lagging edge and increases directional persistence in these cells. Accordingly, this accelerates polarization, but not the expression of stage-specific markers, such as cAR1, during the course of differentiation. Other lagging-edge proteins do not localize asymmetrically in growing cells or noticeably increase polarity when overexpressed (11, 21, 24, 60). Consistent with its role in enhancing polarity, CynA transcription is up-regulated during differentiation, with low levels in growing cells and a peak after 8 h of starvation, when cells acquire maximal polarity and aggregate into mound structures (61, 62) (data are accessible at dictybase.org) (36, 63, 64). Although our data indicate that CynA is important for establishing polarity, other factors also mediate this process, as expected given the redundancy of the signaling and cytoskeletal networks.

Although the underlying mechanisms are still unclear, many models for the establishment of persistent polarity have been proposed. Most have focused on positive feedback loops at the

front of cells involving a number of specific signaling molecules, such as RhoGTPases and PI3K, and a global inhibitory component that prevents activity at multiple sites (65–77). An increasing number of studies have implicated events at the cell rear, such as the local inhibition of signaling activities and force generation through actin depolymerization or Myosin II (78–82). The behavior of CynA shows how positive feedback at the lagging edge can contribute to polarity. CynA clusters act as negative regulators of protrusive activity and, in turn, CynA is forced away from sites of protrusions, resulting in an increased concentration of CynA in surrounding regions. This appears to further restrict the regions that are permissive for protrusions. As the cell becomes increasingly polarized, CynA becomes more tightly clustered at the lagging edge, further reinforcing the restriction of protrusive activity to the leading edge, thereby generating a positive feedback mechanism. It is possible that this combination of both CynA-mediated inhibition of protrusions and the polarity-mediated spatial restriction of CynA clusters is what drives the polarity that is characteristic of differentiated, migrating cells.

## Materials and Methods

A detailed description of the materials and methods used can be found in *SI Materials and Methods*. Plasmids were generated by standard cloning procedures and expressed in *Dicytostelium* cells grown in HL5 media. CynA-null cells were generated by homologous recombination, such that the entire coding sequence was replaced by a drug-resistance cassette. Cells were differentiated in suspension culture with pulses of cAMP or by growing on nonnutrient agar plates as needed and imaged with a 40×/1.3 oil objective and DIC, GFP, and RFP (where applicable) illumination using either a Zeiss Observer.Z1 inverted microscope or Leica DMI6000 inverted microscope equipped with a Yokogawa CSU10 spinning disk. Global stimulation assays were performed using 1 μM cAMP. Chemotaxis assays were performed using a micropipette filled with 10 μM cAMP. Image processing and quantification were done using ImageJ or customized Matlab scripts.

Fig. S1 illustrates in more detail the relationship between CynA localization and other proteins at the lagging edge. Fig. S2 elaborates further on the influence of polarity on the localization, as well as responsiveness to cAMP, of CynA demonstrated in Fig. 2. Fig. S3 shows the phosphoinositide binding of CynA and the localization of CynA truncations and fusions in undifferentiated cells. Fig. S4 depicts the generation of *cynA*⁻ cells and contains additional quantification of the polarity defects associated with disruption or overexpression of CynA as shown in Fig. 4. Fig. S5 shows the localization of front and back proteins in *cynA*⁻ cells and the effects of CynA overexpression on polarity.

**ACKNOWLEDGMENTS.** We thank Dr. M. N. Teruel for providing information in advance of publication; Dr. C. Wolberger for assistance with protein domain annotation; Dr. D. N. Robinson for providing *myo II*⁻ cells and the mCherry-Myosin II construct, as well as for helpful discussions; B. Diplas and Y. Long for generating DNA constructs used in these studies; members of the Johns Hopkins School of Medicine Microscope Core Facility for assistance with microscopy; Drs. M. Iijima, G. Seydoux, and T. Inoue for advice and suggestions; and Drs. Y. Artemenko, H. Cai, Y. Kamimura, and other members of the P.N.D. and Robinson laboratories for helpful suggestions, sharing reagents, and technical advice. This work was supported by National Institutes of Health Grants GM28007 and GM34933 (to P.N.D.), and American Heart Association Fellowship 09PRE2300057 (to K.F.S.).

1. Swaney KF, Huang CH, Devreotes PN (2010) Eukaryotic chemotaxis: A network of signaling pathways controls motility, directional sensing, and polarity. *Annu Rev Biophys* 39:265–289.
2. Haugh JM, Codazzi F, Teruel M, Meyer T (2000) Spatial sensing in fibroblasts mediated by 3′ phosphoinositides. *J Cell Biol* 151(6):1269–1280.
3. Li Z, et al. (2003) Directional sensing requires G beta gamma-mediated PAK1 and PIX alpha-dependent activation of Cdc42. *Cell* 114(2):215–227.
4. Servant G, et al. (2000) Polarization of chemoattractant receptor signaling during neutrophil chemotaxis. *Science* 287(5455):1037–1040.
5. Shi SH, Jan LY, Jan YN (2003) Hippocampal neuronal polarity specified by spatially localized mPar3/mPar6 and PI 3-kinase activity. *Cell* 112(1):63–75.
6. Watton SJ, Downward J (1999) Akt/PKB localisation and 3′ phosphoinositide generation at sites of epithelial cell-matrix and cell-cell interaction. *Curr Biol* 9(8):433–436.
7. Dormann D, Weijer G, Dowler S, Weijer CJ (2004) In vivo analysis of 3-phosphoinositide dynamics during *Dictyostelium* phagocytosis and chemotaxis. *J Cell Sci* 117(Pt 26): 6497–6509.
8. Gassama-Diagne A, et al. (2006) Phosphatidylinositol-3,4,5-trisphosphate regulates the formation of the basolateral plasma membrane in epithelial cells. *Nat Cell Biol* 8(9):963–970.
9. Janetopoulos C, Borleis J, Vazquez F, Iijima M, Devreotes P (2005) Temporal and spatial regulation of phosphoinositide signaling mediates cytokinesis. *Dev Cell* 8(4): 467–477.
10. Martin-Belmonte F, et al. (2007) PTEN-mediated apical segregation of phosphoinositides controls epithelial morphogenesis through Cdc42. *Cell* 128(2):383–397.
11. Moores SL, Sabry JH, Spudich JA (1996) Myosin dynamics in live *Dictyostelium* cells. *Proc Natl Acad Sci USA* 93(1):443–446.
12. Pinal N, et al. (2006) Regulated and polarized PtdIns(3,4,5)P3 accumulation is essential for apical membrane morphogenesis in photoreceptor epithelial cells. *Curr Biol* 16(2): 140–149.
13. von Stein W, Ramrath A, Grimm A, Müller-Borg M, Wodarz A (2005) Direct association of Bazooka/PAR-3 with the lipid phosphatase PTEN reveals a link between the PAR/aPKC complex and phosphoinositide signaling. *Development* 132(7):1675–1686.
14. Li L, Nørrelykke SF, Cox EC (2008) Persistent cell motion in the absence of external signals: A search strategy for eukaryotic cells. *PLoS ONE* 3(5):e2093.
15. Skoge M, et al. (2014) Cellular memory in eukaryotic chemotaxis. *Proc Natl Acad Sci USA* 111(40):14448–14453.
16. Eichinger L, et al. (2005) The genome of the social amoeba *Dictyostelium discoideum*. *Nature* 435(7038):43–57.
17. Lemmon MA (2004) Pleckstrin homology domains: Not just for phosphoinositides. *Biochem Soc Trans* 32(Pt 5):707–711.
18. Park WS, et al. (2008) Comprehensive identification of PIP3-regulated PH domains from *C. elegans* to *H. sapiens* by model prediction and live imaging. *Mol Cell* 30(3): 381–392.
19. Huang YE, et al. (2003) Receptor-mediated regulation of PI3Ks confines PI(3,4,5)P3 to the leading edge of chemotaxing cells. *Mol Biol Cell* 14(5):1913–1922.
20. Yumura S, Mori H, Fukui Y (1984) Localization of actin and myosin for the study of ameboid movement in *Dictyostelium* using improved immunofluorescence. *J Cell Biol* 99(3):894–899.
21. Chung CY, Firtel RA (1999) PAKa, a putative PAK family member, is required for cytokinesis and the regulation of the cytoskeleton in *Dictyostelium discoideum* cells during chemotaxis. *J Cell Biol* 147(3):559–576.
22. Faix J, et al. (2001) Recruitment of cortexillin into the cleavage furrow is controlled by Rac1 and IQGAP-related proteins. *EMBO J* 20(14):3705–3715.
23. Müller-Taubenberger A, et al. (2002) Differential localization of the *Dictyostelium* kinase DPAKa during cytokinesis and cell migration. *J Muscle Res Cell Motil* 23(7-8): 751–763.
24. Iijima M, Devreotes P (2002) Tumor suppressor PTEN mediates sensing of chemoattractant gradients. *Cell* 109(5):599–610.
25. Bosgraaf L, et al. (2005) RasGEF-containing proteins GbpC and GbpD have differential effects on cell polarity and chemotaxis in *Dictyostelium*. *J Cell Sci* 118(Pt 9):1899–1910.
26. Cai H, et al. (2010) Ras-mediated activation of the TORC2-PKB pathway is critical for chemotaxis. *J Cell Biol* 190(2):233–245.
27. Meili R, et al. (1999) Chemoattractant-mediated transient activation and membrane localization of Akt/PKB is required for efficient chemotaxis to cAMP in *Dictyostelium*. *EMBO J* 18(8):2092–2105.
28. Parent CA, Blacklock BJ, Froehlich WM, Murphy DB, Devreotes PN (1998) G protein signaling events are activated at the leading edge of chemotactic cells. *Cell* 95(1):81–91.
29. Sasaki AT, Chun C, Takeda K, Firtel RA (2004) Localized Ras signaling at the leading edge regulates PI3K, cell polarity, and directional cell movement. *J Cell Biol* 167(3): 505–518.
30. Yumura S (1993) Reorganization of actin and myosin II in *Dictyostelium* amoeba during stimulation by cAMP. *Cell Struct Funct* 18(6):379–388.
31. Wang Y, Jiang F, Zhuo Z, Wu XH, Wu YD (2013) A method for WD40 repeat detection and secondary structure prediction. *PLoS ONE* 8(6):e65705.
32. Källberg M, et al. (2012) Template-based protein structure modeling using the RaptorX web server. *Nat Protoc* 7(8):1511–1522.
33. Cullinane AR, Schäffer AA, Huizing M (2013) The BEACH is hot: A LYST of emerging roles for BEACH-domain containing proteins in human disease. *Traffic* 14(7):749–766.
34. Loovers HM, et al. (2006) Distinct roles of PI(3,4,5)P3 during chemoattractant signaling in *Dictyostelium*: A quantitative in vivo analysis by inhibition of PI3-kinase. *Mol Biol Cell* 17(4):1503–1513.
35. Kamimura Y, et al. (2008) PIP3-independent activation of TorC2 and PKB at the cell's leading edge mediates chemotaxis. *Curr Biol* 18(14):1034–1043.
36. Parent CA, Devreotes PN (1996) Molecular genetics of signal transduction in *Dictyostelium*. *Annu Rev Biochem* 65:411–440.
37. Artemenko Y, Swaney KF, Devreotes PN (2011) Assessment of development and chemotaxis in *Dictyostelium discoideum* mutants. *Methods Mol Biol* 769:287–309.
38. Devreotes PN (1994) G protein-linked signaling pathways control the developmental program of *Dictyostelium*. *Neuron* 12(2):235–241.
39. Heid PJ, Geiger J, Wessels D, Voss E, Soll DR (2005) Computer-assisted analysis of filopod formation and the role of myosin II heavy chain phosphorylation in *Dictyostelium*. *J Cell Sci* 118(Pt 10):2225–2237.
40. Lee S, Shen Z, Robinson DN, Briggs S, Firtel RA (2010) Involvement of the cytoskeleton in controlling leading-edge function during chemotaxis. *Mol Biol Cell* 21(11):1810–1824.
41. Lombardi ML, Knecht DA, Dembo M, Lee J (2007) Traction force microscopy in *Dictyostelium* reveals distinct roles for myosin II motor and actin-crosslinking activity in polarized cell movement. *J Cell Sci* 120(Pt 9):1624–1634.

42. Wessels D, et al. (1988) Cell motility and chemotaxis in *Dictyostelium* amebae lacking myosin heavy chain. *Dev Biol* 128(1):164–177.
43. Yoshida K, Soldati T (2006) Dissection of amoeboid movement into two mechanically distinct modes. *J Cell Sci* 119(Pt 18):3833–3844.
44. Bretschneider T, et al. (2004) Dynamic actin patterns and Arp2/3 assembly at the substrate-attached surface of motile cells. *Curr Biol* 14(1):1–10.
45. Xiao Z, Zhang N, Murphy DB, Devreotes PN (1997) Dynamic distribution of chemoattractant receptors in living cells during chemotaxis and persistent stimulation. *J Cell Biol* 139(2):365–374.
46. Iijima M, Huang YE, Luo HR, Vazquez F, Devreotes PN (2004) Novel mechanism of PTEN regulation by its phosphatidylinositol 4,5-bisphosphate binding motif is critical for chemotaxis. *J Biol Chem* 279(16):16606–16613.
47. Rahdar M, et al. (2009) A phosphorylation-dependent intramolecular interaction regulates the membrane association and activity of the tumor suppressor PTEN. *Proc Natl Acad Sci USA* 106(2):480–485.
48. Booth AM, et al. (2006) Exosomes and HIV Gag bud from endosome-like domains of the T cell plasma membrane. *J Cell Biol* 172(6):923–935.
49. Fang Y, et al. (2007) Higher-order oligomerization targets plasma membrane proteins and HIV gag to exosomes. *PLoS Biol* 5(6):e158.
50. Nguyen DG, Booth A, Gould SJ, Hildreth JE (2003) Evidence that HIV budding in primary macrophages occurs through the exosome release pathway. *J Biol Chem* 278(52):52347–52354.
51. Shen B, Fang Y, Wu N, Gould SJ (2011) Biogenesis of the posterior pole is mediated by the exosome/microvesicle protein-sorting pathway. *J Biol Chem* 286(51):44162–44176.
52. Shen B, Wu N, Yang JM, Gould SJ (2011) Protein targeting to exosomes/microvesicles by plasma membrane anchors. *J Biol Chem* 286(16):14383–14395.
53. Baumann T, Affentranger S, Niggli V (2012) Evidence for chemokine-mediated coalescence of preformed flotillin hetero-oligomers in human T-cells. *J Biol Chem* 287(47):39664–39672.
54. Ludwig A, et al. (2010) Flotillin microdomains interact with the cortical cytoskeleton to control uropod formation and neutrophil recruitment. *J Cell Biol* 191(4):771–781.
55. Neumann-Giesen C, et al. (2004) Membrane and raft association of reggie-1/flotillin-2: Role of myristoylation, palmitoylation and oligomerization and induction of filopodia by overexpression. *Biochem J* 378(Pt 2):509–518.
56. Rossy J, Schlicht D, Engelhardt B, Niggli V (2009) Flotillins interact with PSGL-1 in neutrophils and, upon stimulation, rapidly organize into membrane domains subsequently accumulating in the uropod. *PLoS ONE* 4(4):e5403.
57. Solis GP, et al. (2007) Reggie/flotillin proteins are organized into stable tetramers in membrane microdomains. *Biochem J* 403(2):313–322.
58. Nakajima A, Ishihara S, Imoto D, Sawai S (2014) Rectified directional sensing in long-range cell migration. *Nat Commun* 5:5367.
59. Wang MJ, Artemenko Y, Cai WJ, Iglesias PA, Devreotes PN (2014) The directional response of chemotactic cells depends on a balance between cytoskeletal architecture and the external gradient. *Cell Reports* 9(3):1110–1121.
60. Kriebel PW, Barr VA, Parent CA (2003) Adenylyl cyclase localization regulates streaming during chemotaxis. *Cell* 112(4):549–560.
61. Parikh A, et al. (2010) Conserved developmental transcriptomes in evolutionarily divergent species. *Genome Biol* 11(3):R35.
62. Rot G, et al. (2009) dictyExpress: A *Dictyostelium discoideum* gene expression database with an explorative data analysis web-based interface. *BMC Bioinformatics* 10:265.
63. Chen L, et al. (2003) Two phases of actin polymerization display different dependencies on PI(3,4,5)P3 accumulation and have unique roles during chemotaxis. *Mol Biol Cell* 14(12):5028–5037.
64. Garcia GL, Parent CA (2008) Signal relay during chemotaxis. *J Microsc* 231(3):529–534.
65. Butty AC, et al. (2002) A positive feedback loop stabilizes the guanine-nucleotide exchange factor Cdc24 at sites of polarization. *EMBO J* 21(7):1565–1576.
66. Charest PG, Firtel RA (2006) Feedback signaling controls leading-edge formation during chemotaxis. *Curr Opin Genet Dev* 16(4):339–347.
67. Cheng PL, Poo MM (2012) Early events in axon/dendrite polarization. *Annu Rev Neurosci* 35:181–201.
68. Inoue T, Meyer T (2008) Synthetic activation of endogenous PI3K and Rac identifies an AND-gate switch for cell polarization and migration. *PLoS ONE* 3(8):e3068.
69. Kozubowski L, et al. (2008) Symmetry-breaking polarization driven by a Cdc42p GEF-PAK complex. *Curr Biol* 18(22):1719–1726.
70. Meinhardt H (1999) Orientation of chemotactic cells and growth cones: Models and mechanisms. *J Cell Sci* 112(Pt 17):2867–2874.
71. Meinhardt H, Gierer A (2000) Pattern formation by local self-activation and lateral inhibition. *BioEssays* 22(8):753–760.
72. Srinivasan S, et al. (2003) Rac and Cdc42 play distinct roles in regulating PI(3,4,5)P3 and polarity during neutrophil chemotaxis. *J Cell Biol* 160(3):375–385.
73. Wang F (2009) The signaling mechanisms underlying cell polarity and chemotaxis. *Cold Spring Harb Perspect Biol* 1(4):a002980.
74. Wedlich-Soldner R, Altschuler S, Wu L, Li R (2003) Spontaneous cell polarization through actomyosin-based delivery of the Cdc42 GTPase. *Science* 299(5610):1231–1235.
75. Weiner OD, et al. (2002) A PtdInsP(3)- and Rho GTPase-mediated positive feedback loop regulates neutrophil polarity. *Nat Cell Biol* 4(7):509–513.
76. Wu CF, Lew DJ (2013) Beyond symmetry-breaking: Competition and negative feedback in GTPase regulation. *Trends Cell Biol* 23(10):476–483.
77. Xu J, et al. (2003) Divergent signals and cytoskeletal assemblies regulate self-organizing polarity in neutrophils. *Cell* 114(2):201–214.
78. Cramer LP (2010) Forming the cell rear first: Breaking cell symmetry to trigger directed cell migration. *Nat Cell Biol* 12(7):628–632.
79. Mseka T, Cramer LP (2011) Actin depolymerization-based force retracts the cell rear in polarizing and migrating cells. *Curr Biol* 21(24):2085–2091.
80. Verkhovsky AB, Svitkina TM, Borisy GG (1999) Self-polarization and directional motility of cytoplasm. *Curr Biol* 9(1):11–20.
81. Vicente-Manzanares M, Koach MA, Whitmore L, Lamers ML, Horwitz AF (2008) Segregation and activation of myosin IIB creates a rear in migrating cells. *J Cell Biol* 183(3):543–554.
82. Yam PT, et al. (2007) Actin-myosin network reorganization breaks symmetry at the cell rear to spontaneously initiate polarized cell motility. *J Cell Biol* 178(7):1207–1221.
83. Ruppel KM, Uyeda TQ, Spudich JA (1994) Role of highly conserved lysine 130 of myosin motor domain. In vivo and in vitro characterization of site specifically mutated myosin. *J Biol Chem* 269(29):18773–18780.
84. Faix J, Kreppel L, Shaulsky G, Schleicher M, Kimmel AR (2004) A rapid and efficient method to generate multiple gene disruptions in *Dictyostelium discoideum* using a single selectable marker and the Cre-loxP system. *Nucleic Acids Res* 32(19):e143.
85. Pitt GS, et al. (1992) Structurally distinct and stage-specific adenylyl cyclase genes play different roles in *Dictyostelium* development. *Cell* 69(2):305–315.
86. Nagasaki A, de Hostos EL, Uyeda TQ (2002) Genetic and morphological evidence for two parallel pathways of cell-cycle-coupled cytokinesis in *Dictyostelium*. *J Cell Sci* 115(Pt 10):2241–2251.
87. Thévenaz P, Ruttimann UE, Unser M (1998) A pyramid approach to subpixel registration based on intensity. *IEEE Trans Image Process* 7(1):27–41.